Asian Journal of Chemistry; Vol. 29, No. 6 (2017), 1206-1214

ASIAN JOURNAL OF CHEMISTRY

https://doi.org/10.14233/ajchem.2017.20374

Synthesis and Characterization of Graphene/Polyaniline Nanocomposite Using Green Solvents

K.R. SEBOGODI[1], K. KOTLHAO[2] and M.J. KLINK[3,*]

[1]Department of Chemistry, Faculty of Agriculture, Science and Technology, North-West University (Mafikeng Campus), Private Bag X2046, Mmabatho 2735, South Africa
[2]Department of Chemistry, Faculty of Applied and Computer Sciences, Vaal University of Technology, Private Bag X021, Vanderbijl Park 1900, South Africa
[3]Department of Chemistry/Biotechnology, Faculty of Applied and Computer Sciences, Vaal University of Technology, Private Bag X021, Vanderbijl Park 1900, South Africa

*Corresponding author: Fax: +27 16 950 9794; Tel: +27 16 950 7507; E-mail: michaelk1@vut.ac.za

Received: 26 October 2016; *Accepted*: 16 February 2017; *Published online*: 10 April 2017; AJC-18327

Graphene/polyaniline (GR/PANI) nanocomposite materials were synthesized in four different imidazolium based green ionic liquids, 1-butyl-2,3-dimethylimidazolium tetraflouroborate, 1-butyl-3-methylimidazolium tetraflouroborate, 1-butyl-3-methylimidazolium hexaflourophosphate and 1-butyl-3-methylimidazolium *bis*(triflouromethylsulfonyl) imide. Successful synthesis of the GR/PANI nanocomposite was confirmed by scanning electron microscopy (SEM), energy dispersive X-ray (EDX), Fourier transformed infrared spectroscopy (FTIR), UV-visible spectroscopy (UV-Vis), X-ray diffractometer (XRD) and thermogravimetric analysis (TGA). FTIR and UV-visible results successfully confirmed the incorporation of polyaniline into the graphene/polyaniline structures. The SEM micrographs of the nanocomposites synthesized in ionic liquids showed that the polyaniline material were nucleated, aggregated or evenly distributed in between the graphene sheets depending on ionic solvent used, unlike a thick wavy films or passivated layer of the PANI nano material formed on the graphene sheet in the organic solvent. The XRD gave crystal sizes ranged between 89-950 nm and 29-250 nm for composites synthesized in ionic liquids and organic solvents respectively. Larger crystal size in ionic liquids was attributed to easy dissolution of starting material and electrostatic interaction between molecules. Energy dispersive X-ray and thermogravimetric analysis showed that the graphene/polyaniline nanocomposites synthesized in the presence of ionic liquids have similar properties to those synthesized in organic solvents. The photochemical and electrochemical properties of the ionic and organic solvent synthesized GR/PANI nanocomposite in catalysis, sensor and energy devices will be subject for future study.

Keywords: Green chemistry, Ionic liquids, GR/PANI nanocomposite.

INTRODUCTION

Our lives are dependent on materials and/or technology, which unfortunately come with a tremendously huge luggage of "dirt". That is its production involves the usage of chemicals, which could be hazardous (*i.e.* volatile organic solvents) towards both human beings and the environment [1].

A memorandum of understanding was signed by different nations to address the issue of hazards they are faced with and this gave birth to what is known as "Green Chemistry". This green chemistry has been addressed through outreach initiatives, research, implementation and education. In terms of research, Green Chemistry has been practiced in several industries such as in solvents, catalysis, polymers, renewables, analytical methods development, design of safer chemicals and the development of synthetic methods. Therefore, to ensure a cleaner future, chemists went back to the drawing board to re-evaluate chemical processes-with the guidance of the twelve principles of green chemistry and came-up with several strategies of producing a "cleaner technology". When looking to the solvent industry, these strategies include the four mainly praised, which are namely, solvent free synthesis, use of water as a solvent, use of supercritical fluids and most recently the use of ionic liquids as solvents [2]. Each of the first three strategies had some problems whereas the fourth one (which is the use of ionic liquids as solvent) is increasingly being applied in the chemical and synthetic industries. This is because ionic liquids are not only green, but they also offer efficient product abstraction, have no or minimal waste, meaning that they have no or minimal disposal costs and have remarkable properties [2].

Ionic liquids are salts, which are fluid over a varied temperature range, or liquid salts consisting of ion pairs [3-7]. These liquids are made-up of two ions in which one or both

ions could be large. The exponential growth of interest in ionic liquids is due to their properties such as low/negligible vapour pressures, high viscosities, thermal stability and low melting points [3-7]. These properties enable them to be used as solvents for inorganic, organic and polymeric materials synthesis, electrochemical applications, liquid phase extraction and catalysis for clean technology [8].

Ionic liquids are sometimes termed "designer solvents", because they can be designed to achieve certain specific properties. Their miscibility and thermal stability depends on the anion, while their viscosity and density depend on the side chain length in the cation. This means that depending on the choice of ions, it is possible to prepare ionic liquids at or below room temperature, for example ethylammonium nitrate $[EtNH_3][NO_3]$ has a melting point of 12 °C. The mutual electrostatic forces (of charged particles) in these liquids makes them miscible with polar solvents while their solubility in less polar solvents is determined by the alkyl chain in the cation, *e.g.* substituting PF_6^- with BF_4^- increases the solubility in water and changing 1-alkyl chain from 1 to 10 on 1-alkyl-3-methylimidazolium hexafluorophosphate, $[CnMIm][PF_6]$ makes it immiscible in water [4,6]. Another important characteristic of these liquids is that they are recyclable, so that minimal environmental contamination occurs during their production [3,6].

In this work, graphene/polyaniline nanocomposite was synthesized in four different imidazolium based ionic liquids [1-butyl-2,3-dimethylimidazolium tetraflouroborate, 1-butyl-3-methylimidazolium tetraflouroborate, 1-butyl-3-methylimidazolium hexaflourophosphate and 1-butyl-3-methylimidazolium *bis*(triflouromethylsulfonyl)imide] and characterized using different spectroscopy and microscopic techniques. Particle sizes and morphology are compared with those synthesized using organic solvents. The motivation to this study is to come up with alternative solvents (green solvents) for graphene/polyaniline synthesis, which are environmentally friendly and will produce GR/PANI that compares favourably or better in terms of yield, physico-chemical properties and applications to those synthesized using conventional solvents.

EXPERIMENTAL

Graphite flake, ammonium peroxydisulfate, 1-butyl-3-methyl imidazolium *bis*(trifluoromethylsulfonyl) imide, 1-butyl-2.3-dimethylimidazolium tetrafluoroborate were purchased from Sigma-Aldrich. Aniline hydrochloride, 1-butyl-3-methylimidazolium hexafluorophospate were purchased from Fluka, Hydrogen peroxide 30 % was purchased at LAB CHEM and hydrochloric acid 32 %, sulphuric acid 95-99 %, potassium permanganate, sodium nitrate, ethanol absolute, hydrazonium hydroxide were purchased at Merck.

Preparation of polyaniline (PANI): Polyaniline nanofibers were synthesized by a rapid mixing polymerization method. The two solutions, one made-up of hydrochloric acid and aniline hydrochloride and the other one made-up of hydrochloric acid and ammonium peroxydisulfate were mixed with each other under vigorous stirring for 4 h. The precipitate was collected by filtration, washed with water and ethanol and dried in a vacuum oven [9].

Preparation of graphene: The graphene oxide (GO) was synthesized by using the modified Hummers method. Generally, graphite and sodium nitrate were mixed and stirred in a beaker containing concentrated H_2SO_4 for 30 min in an ice bath. A few grams of potassium permanganate were added slowly to the suspension while under stirring. The mixture was removed from the ice bath and stirred at room temperature overnight. This was followed by addition of water and stirring of the suspension for 24 h while keeping the temperature at 98 °C. The following day 30 % hydrogen peroxide was added to the solution, followed by purification (with 5 % HCl and centrifugation) and drying. Finally the graphene was prepared by reducing graphene oxide with hydrazine monohydrate at 98 °C [10].

Preparation of graphene/polyaniline (PANI) composites: The nanocomposites were synthesized *via* an *in situ* intercalative polymerization technique. Aniline hydrochloride was diluted in different ionic liquids or organic solvents and graphene oxide was added into this mixture which was then sonicated for 30 min and stirred vigorously using a magnetic stirrer for another 30 min (in order to separate the graphene oxide layers) and then the procedure of synthesizing polyanilne nanofibers was followed. After washing, the composites were dried in a vacuum oven. The graphene oxide in the composite was reduced by hydrazine monohydrate at 98 °C and the composites were washed with distilled water. This was followed by reoxidation/reprotonation of PANI-f and lastly drying [9].

The obtained nanocomposite was characterized using different spectroscopic and microscopic techniques. The UV-visible spectra were recorded on a Perkin Elmer Lamdab 750 S UV/visible spectrometer within the wavelength region of 100 to 1000 nm using the KBr dispersed samples. Field emission scanning electron microscope (FESEM) images were obtained from JEOL JSM 6000 LV (Japan), energy dispersive X-ray spectra (EDX) were obtained from NORAN VANTAGE (USA), while the XRD analysis was done using a back loading preparation method. The sample was analyzed using a PANalytical X'Pert Pro powder diffractometer (Netherland) with X'Celerator detector and variable divergence- and receiving slits with Fe filtered Co-Kα radiation.

RESULTS AND DISCUSSION

The results of the microscopic and the spectroscopic analysis *vis a vis* scanning electron microscopy (SEM), energy dispersive X-ray analysis (EDAX), X-ray diffractometer (XRD), Fourier transform infrared spectroscopy (FTIR), ultraviolet visible spectroscopy (UV-vis) and thermogravimetric analysis (TGA) of the different nanosized graphene/polyaniline composites synthesized in the different ionic liquids and conventional solvents are presented in Figs. 1-7.

Scanning electron microscopy: The SEM micrographs of the GR, PANI and GR/PANI nanocomposites are presented in Figs. 1-3. Fig. 1 presents the SEM images of the synthesized GR and PANI alone, while Figs. 2 and 3 represent the SEM images GR/PANI nanocomposites synthesized in different solvents. Fig. 1a is the SEM micrographs of PANI nanostructures synthesized in an aqueous solution of HCl (1 M). The nanostructures are in a fiber form and nucleated because

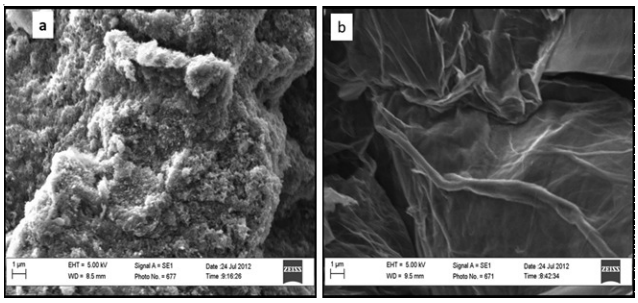

Fig. 1. (a) SEM micrograph of polyaniline (PANI) nanofibers prepared in 1 M HCl and (b) the SEM micrograph of the synthesized graphene (GR)

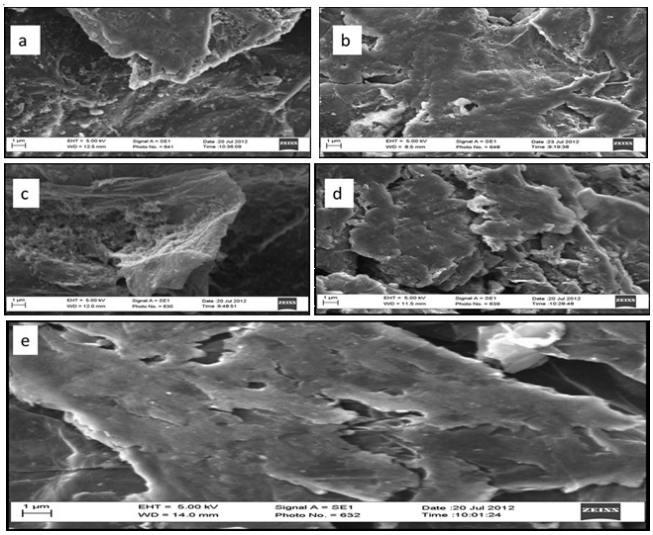

Fig. 2. SEM micrographs of the GR/PANI nanocomposites synthesized in organic solvents such as in (a) toluene, (b) dimethyl sulfoxide (DMSO), (c) dichloromethane (DMC), (d) acetone and (e) tetrahydrofuran (THF)

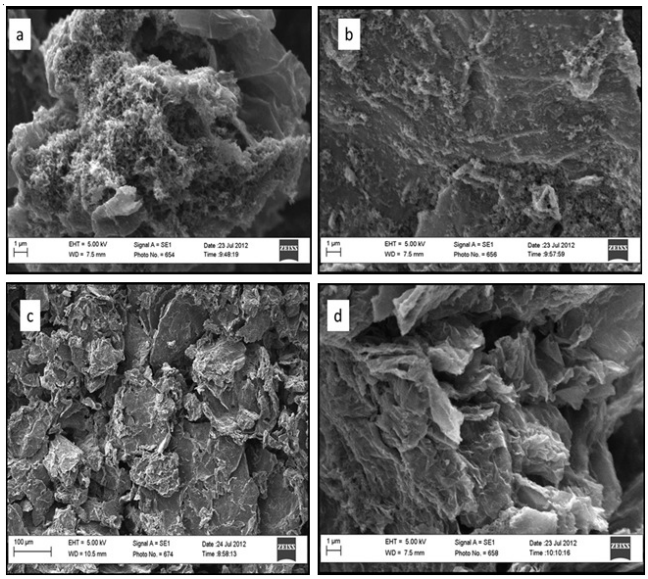

Fig 3. SEM micrograph of GR/PANI synthesized in imidazolium based ionic liquids such as in (a) 1-butyl-3-methyl imidazolium hexaflourophosphate[BMIM][PF_6], (b) 1-butyl-3-methyl imidazolium *bis*(trifluoromethyl sulfonyl) imide [BMIM][NTF_2], (c) 1-butyl-2,3-dimethylimidalium tetraflouroborate [BDMIM][BF_4] and 1-butyl-3-methyl imidazolium tetrafluoroborate [BMIM][BF_4]

they were formed under vigorous stirring [11]. Fig. 1b shows the image of graphene, which was reduced in water as a dispersing agent. This picture showed that graphene is wrinkled nanofibers similar to carbon nanotubes (CNTs) and this may have happened during the reduction because reduction of graphene oxide causes the material to agglomerate irreversibly and this agglomeration may have caused the thin monolayer sheets of graphite to get wrinkled [12].

Scanning electron micrographs (Fig. 2a-e) of graphene/polyaniline nanocomposites which were synthesized in different conventional organic solvents namely toluene, dimethyl sulfoxide (DMSO), dichloromethane (DMC), acetone and tetrahydrofuran (THF) respectively. All these solvents are polar aprotic except for toluene, which is a non-polar solvent. The SEM images of GR/PANI nanocomposites synthesized in toluene (Fig. 2a) showed well spread, slippery and wafers/flakes form of the PANI on the GR sheets. Similar configurations were obtained for the nanocomposites synthesized in the DMSO (Fig. 2b), acetone (Fig. 2d) and THF (Fig. 2e). It is therefore important to state that the graphene nanoparticles provided a porous, large surface area that favours the spread of the PANI nanoparticles. The wafer-like PANI may have been caused by the miscibility of the solvents (DMSO, acetone and THF) in water. During the *in situ* polymerization the initiator was dissolved in a diluted HCl and if the solvents are water miscible it means that there is a possibility that the new polymers is formed on top of the pre-formed ones and this caused agglomeration of particles [11]. In the DMC synthesized composites (Fig. 2c), the GR sheets formed cone-like structures in which the loosely packed nanofibrillar PANI is beautifully embedded. However, the polarity and impact of solvent on the PANI in the nanocomposite cannot be overemphasized. For example, even though all the images in Fig. 2 indicated a wafers/flakes form of the PANI on the GR sheets but the extent of this flakes is different from solvent to solvent. For example, PANI polymers in the composites synthesized in toluene and DMC was a combination of both aggregated films and nucleated nanoparticles probably because the polymer was formed through the interfacial polymerization at the interface between water and the organic solvent and then migrates to the organic phase after formation [11,13-15]. In addition, polymers in the toluene synthesized composites are a bit nucleated probably due to the non-polar nature of the solvent which absolutely affects its miscibility with water.

The GR/PANI nanocomposites were also synthesized in different immidazolium based ionic liquids and the SEM micrographs presents in Fig. 3. There is a distinctive structural differences between the GR/PANI images obtained in the organic solvent (Fig. 2) and those obtained in the ionic liquids (Fig. 3). For example, while a thick film and very wavy flakes of PANI polymers were formed in the GR/PANI nanocomposite in organic solvent, an aggregated, nucleated and evenly distributed PANI particles are formed on the GR sheet using ionic liquids (Fig. 3).

The SEM micrographs shows that the PANI in the composites synthesized in 1-butyl-3-methylimidazolium hexaflourophosphate (Fig. 3a) form a nucleated and aggregated nanoparticles which are embedded right on the surface of the

cone-like graphene sheet, while the one synthesized in 1-butyl-3-methyl imidazolium *bis*(trifluoromethyl sulfonyl)imide is homogeneously and evenly distributed in both the pores and on the GR surface (Fig. 3b). The distribution of the particles as observed in Fig. 3a and 3b could be due to the strong ionic interactions between amino group of the PANI particles and the imidazolium ion of the solvents employed in the synthesis. Similar ionic or electrostatic interactions were reported for aggregated and evenly distributed metal nanoparticles respectively on acidic functionalized carbon nanotubes [16]. It could also be due to the presence of the phosphate and the sulphonyl group in the solvents, which increases the acidic nature of the medium, protonating the amino group of the PANI and making it readily available for ionic interactions with the solvents and the graphene particles. The SEM image of the composites synthesized in 1-butyl-2,3-dimethyl tetrafluoroborate (Fig. 3c) and 1-butyl-3-methylimidazolium tetrafluoroborate (Fig. 3d) showed that the polymers form aggregated flakes in Fig. 5c and embedded nanoparticles in Fig. 3d. This conformation could be attributed to the borate ions present in these ionic liquids [17].

In brief, it is clear from the SEM images that the GR/PANI nanocoposite gave different morphology in the ionic liquid and the conventional organic solvents respectively. While a nucleated, aggregated or evenly distributed PANI molecules in between the graphene sheets were obtained using ionic liquids depending on ionic solvent used, a thick wavy films or passivated layer of the PANI nano material were formed on the graphene sheet in the organic solvent. The extent to which this GR/PANI nanocomposite morphology affects the photochemical and electrochemical properties of the synthesized material in catalysis, sensor and energy devices will be subject for future study.

Energy dispersive X-ray (EDX) analysis: The EDX profile showing the weight percentages of different elements present in the synthesized PANI, GR, GR/PANI in toluene and GR/PANI in 1-butyl-3-methylimidazolium hexaflourophosphate [BMIM][PF_6] are shown in Fig. 4.

Generally, carbon is the most prominent element in all the samples indicating the polymeric nature of the PANI and GR. Theoretically, the constituents of this PANI should be carbon, hydrogen, nitrogen and chlorine, while graphene is said to be the sp^2 hybridized monolayer of carbon atoms which are arranged in a hexagonal honey-comb structure [9,22], this definition tells us that there shouldn't be any other element present in the graphene sample. However, the presence of oxygen in PANI is probably due to traces of adsorbed moisture from the atmosphere or PANI sample not properly dried after synthesis. Its (oxygen) prominence in GR can be attributed to incomplete reduction of the carbonyl and the hydroxyl groups of graphene oxide to graphene during synthesis. Similar reasons can be given for the presence of oxygen in GR/PANI synthesized in either toluene or 1-butyl-3-methylimidazolium hexaflourophosphate. Presence of chlorine in PANI is attributed to the polymerization of aniline chloride in an aqueous solution of 1 M HCl; while traces of sulphur in some of the samples have been attributed to the trace quantity of this element in the starting materials. Nitrogen is not detected since the instrument was run under nitrogen gas [9,17].

The EDX profiles of GR/PANI nanocomposites synthesized using other organic and ionic solvents (not shown) indicate the presence of carbon atoms between 71 and 74 %, while their chlorine content is far lower than the one in PANI alone. This is due to the fact that these samples were prepared using the *in situ* oxidative-reduction/re-oxidation-redoping process. This means that the doping degree of the polymer within the composites was decreased by the reducing agent (hydrazine hydrate) while trying to reduce graphene oxide [9,18]. Hydrazine hydrate is a strong reducing agent, so its addition to the GO/PANI composites not only reduces the graphene oxide but also reduces PANI.

X-ray diffractometer (XRD) analysis: Fig. 5 presents the XRD spectra of the synthesized PANI, GR, GR/PANI in toluene and GR/PANI in 1-butyl-3-methylimidazolium hexaflourophosphate [BMIM][PF_6]. The XRD profiles of GR/PANI in other organic and ionic liquid solvents were also obtained (not shown). X-ray diffraction measures the interlayer spacings and the crystallite sizes of the samples.

The XRD spectrum of polyaniline nanofibers shows 2θ peaks at 9.37, 16.00 and 25.72°, respectively. The interlayer spacing (d) for this nanofibers was calculated according to Braggs law [19-21]:

$$n\lambda = 2d\ \mathrm{Sin}\theta \quad (1)$$

The 2θ value for the most prominent peak was used in estimating the interlayer spacing value (d). From eqn. 1, interlayer spacing of 0.346 nm was obtained for the synthesized PANI molecules therefore confirming its nano nature. In literature, the XRD spectrum of graphene oxide shows a 2θ peak between 11.6-13.1°, which corresponds to the interlayer spacing of 0.72 nm [9,22,23]. This huge spacing had been assigned to the presence of oxygen containing functional groups and water within the graphene oxide. In this study, the XRD of the synthesized GR gave interlayer spacing as low as 0.353 nm. This indicates successful recovery of the sp^2 conjugated carbon atoms and the crystallinity of GR [8,18]. However, the 2θ peaks

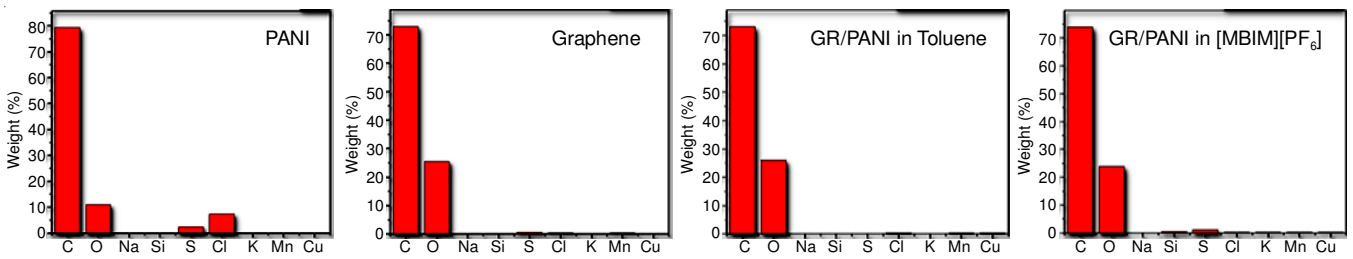

Fig. 4. EDX profiles of PANI, GR and GR/PANI synthesized in toluene and [BMIM][PF_6] respectively

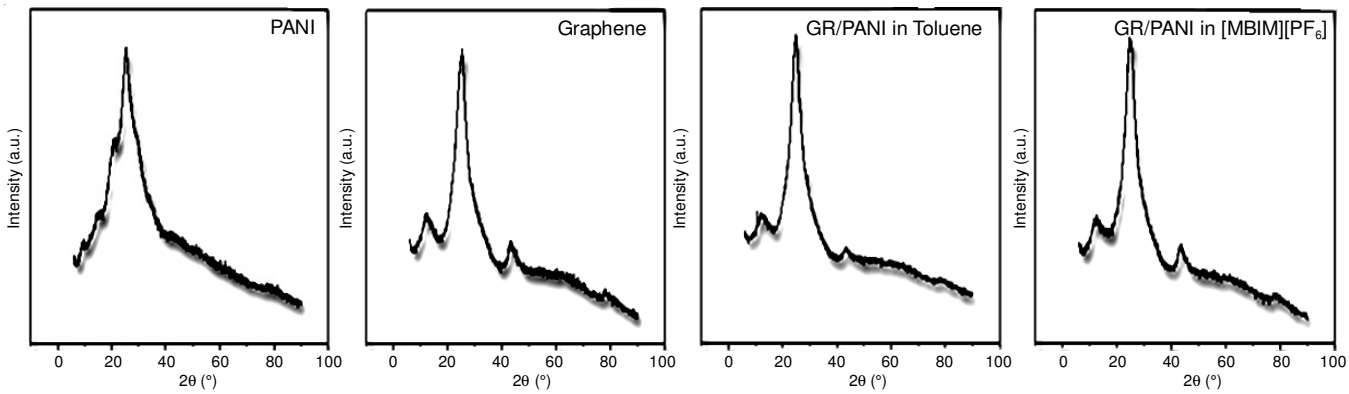

Fig. 5. XRD of PANI, GR and GR/PANI nanocomposites synthesized in toluene and [BMIM][PF_6]

at 12.09° suggests that the GR is not fully reduced which is in agreement with the EDX results. The 2θ at about 25.06 and 42.9° indicate the graphite-like structures of the GR [22].

The XRD spectra of the GR/PANI nanocomposites synthesized in the different solvents (not shown) gave interlayer spacing ranging from 0.355-0.360 nm (Table-1). The peaks of these composites, which are similar to that of PANI (at 2θ 16.00 and 24°) indicate the interaction between the graphene and polyaniline but the 2θ at about 43° could be correlated to the reduced PANI. The PANI was initially in the form of a conducting emeraldine salt but after reduction by hydrazine monohydrate it changed to the insulating emeraldine base [23]. The results are in good agreement with the EDX where the weight percentage of chlorine present in the composites is far low compared with that of PANI alone.

Furthermore, XRD patterns were used to determine the crystallite size of samples using the Scherrer's equation [24,25]:

$$T = \frac{K\lambda}{\beta\cos\theta} \quad (2)$$

where: T is the crystallite size (nm), K, shape factor for an average crystallite (0.9), λ is the XRD wavelength (nm), β is the width at half maximum of crystallite peak (radians) and θ is Bragg's angle of the XRD peak.

The most intense peaks from the XRD spectrum were used to calculate the crystallite size (T) (Table-1). The crystallite size for GR was estimated to be 3.85 nm, which corresponds to the value reported in the literature [24,26]. For the synthesized PANI nanopolymers, the crystallite size was found to be 60.26 nm, which also agreed with values reported in literature [25]. The GR/PANI composites synthesized using different solvents (organic and ionic liquids) have crystal size ranging from about 30 to about 250 nm depending on the solvent used (Table-1). It can be inferred from the table that the crystallite sizes of the composites synthesized in organic solvents are smaller compared to those of the composite synthesized in ionic liquids. Aside the normal molecular interaction *vis-à-vis* hydrogen bonding between the PANI backbone and the O=C-O of GR and π-π interaction between the two constituents of the nanocomposites [27-30] envisaged for the GR/PANI molecules in either the organic solvent or ionic liquids, the larger nanocomposite sizes recorded in the ionic liquids can be attributed to additional factors such as (i) the presence of acidic functional groups such as sulphonic, phosphate and borate groups which enhances the dissolution and distribution of the PANI in and out of the pores of GR base and on the surface of the GR sheet. (ii) strong ionic or electrostatic interactions between the protonated PANI nanopolymers and the GR nanoparticles leading to nucleated and sometimes, aggregated particles embedded in, or on the surface of the GR sheet. It was also observed for the GR/PANI nanocomposite from the ionic liquids that the stronger the acidic groups, the larger the sizes of the GR/PANI nanocomposite since there is better dissolution and distributions of particles. For example, the nanocomposite crystallite sizes are smaller in borate containing ionic liquids (about 89 nm) compared with those containing sulfonic HSO_3^- group (about 947 nm) and phosphate group (about 253 nm) since the borate anion is weaker.

Fourier transformed infrared spectroscopy (FTIR) analysis: The FTIR spectra of GR, PANI and GR/PANI nanocomposites in toluene and [BMIM][PF_6] are presented in Fig. 6. The samples were run in the wavelength range between 4000 and 400 cm^{-1}. The FTIR spectrum of graphene oxide

TABLE-1
XRD DATA USED FOR CALCULATING THE INTERLAYER SPACING AND CRYSTALLITE SIZE OF DIFFERENT SAMPLES

Compound	2θ	θ	d = nλ/(2 Sin θ)	T = Kλ/(β Cos θ)
GR	25.24150	12.62075	0.353	3.854
PANI	25.72370	12.86185	0.346	60.262
GR/PANI in toluene	24.75930	12.37965	0.359	43.500
GR/PANI in DMSO	24.88557	12.42779	0.358	29.765
GR/PANI in DMC	24.66280	12.33140	0.360	31.056
GR/PANI in acetone	24.90390	12.42785	0.358	29.890
GR/PANI in THF	24.90390	12.45195	0.357	30.535
GR/PANI in [BMIM][PF_6]	24.66280	12.33140	0.361	253.436
GR/PANI in [BMIM][NTF_2]	24.90390	12.45195	0.357	946.600
GR/PANI in [BDMIM][BF_4]	25.09680	12.54840	0.355	89.335
GR/PANI in [BMIM][BF_4]	25.00400	12.50020	0.356	89.319

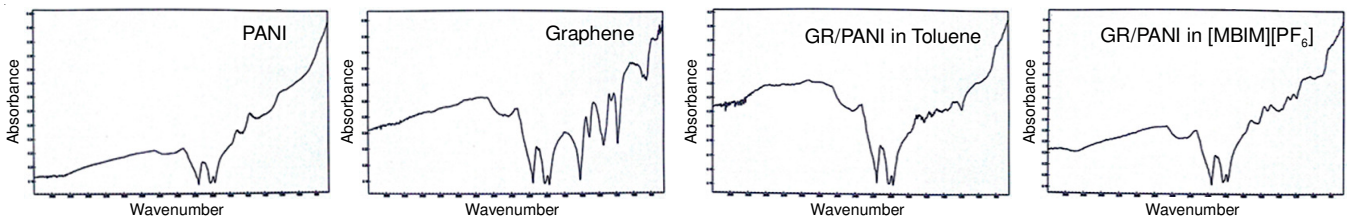

Fig. 6. FTIR graphs of (a) GR, (b) PANI, GR/PANI nanocomposites synthesized in (c) toluene and (d) [BMIM][PF_6]

(GO) (not shown) consists of bands at around 1701 and 1273 cm^{-1}, which are due to the C=O and C-O stretching mode respectively, bands in 3372 cm^{-1} region are due to the O-H stretching of –COOH, peaks at 1650-1450 cm^{-1} attributed to the C=C in the benzene ring and lastly the C-H stretch band near the 3000 cm^{-1} [9,27-31]. Theoretically, it was reported that graphene oxide consists of oxygen moieties such as hydroxyl, epoxy (which are located on the sp^3 carbons in the basal plane), carboxyl and carbonyl (located on the sp^2 carbons) groups [9,22]. However, the FTIR spectrum of GR (Fig. 6a) showed a diminished epoxy and hydroxyl peaks at around 1700 to 1056 cm^{-1} respectively due to the reduction and deoxygenating of graphene oxide with hydrazine monohydrate. Bands at around 1650 is attributed to C=C vibrations in the phenyl structure, while peaks at around 1713 and 1261 are due to C=O of COOH and C-O of C-O-C/C-O-H groups respectively. These characteristic bands remain in the GR sample after graphene oxide reduction due to the inability of hydrazine to reduce them [29]. Graphene itself is defined as a two dimensional honey comb structure of sp^2 carbon [9,22]. This definition suggests that there should be no other functional groups that should/could be found in the structure of graphene. This could only be true if the graphene is produced using the bottom-up synthetic methods [32-34]. In contrary, this study employed a top-down method involving synthesizing graphene oxide and reducing it with hydrazine monohydrate, which results in other functional groups other than carbon alone as depicted in the FTIR spectrum obtained (Fig. 6a). The advantage of using hydrazine as a reductant in this work is because it has no reactivity with the water which was used as a medium of reaction, while the disadvantage is that it had been reported that hydrazine is in capable of removing all the oxygen moieties which are located on the edges of the graphene (carbonyl and the carboxyl groups), therefore leaving behind the oxygen moieties found on the synthesized graphene samples [29,35].

Spectroscopic characterization of the synthesized polyaniline emeraldine salt (PANI) was also investigated using FTIR (Fig. 6b). Some characteristics peaks, which are typical of PANI are observed and presented in Table-2. Bands around 1500, 1600, 1300, 1100 and 800 cm^{-1} are attributed to C=C bond of benzoid, C=C bond of quinoidal, C-N of secondary amine stretch, C-H in-plane bending and C-H out of plane bending respectively [9,11,28,30,31,36-38].

After the *in situ* polymerization of polyaniline onto the surface of graphene using both the organic solvent and the ionic liquids, the resulting GR/PANI nanocomposites were elucidated for structural changes using FTIR spectroscopic. Fig. 6c and 6d are the spectra obtained for the nanocomposite synthesized in toluene and [BMIM][PF_6] respectively, while the spectra information are presented in Table-2. FTIR bands

TABLE-2
FTIR SPECTRAL DATA FOR GRAPHENE OXIDE, GR, PANI AND GR/PANI COMPOSITE

Compound	Wavenumber (cm^{-1})	Assignment
GO	1701.114	C=O of COOH
	1272.962	C–O of C–O–/C–OH
	3372.186	O-H of COOH & intercalated H_2O
	1649.991	C=C of benzene ring
	2915.277	C–H stretch
GR	1649.991	C=C of phenyl stretch
	1712.921	C=O of COOH
	1261.349	C–O of C–O–C/C–OH
PANI	1621.235	C=C of quinoid stretch
	1515.794	C=C of benzoid stretch
	1352.841	C–N of secondary amine
	1193.082	C–H in-plane bending
	841.614	C–H out of plane bending
GR/PANI nanocomposites synthesized in toluene	1618.040	C=C of quinoid ring
	1538.573	C=C of benzoid ring
	1349.646	C–N of secondary amine
	1289.397	C=N (–N=Quinoid=N–)
	1196.278	C–H in-plane bending
	771.320	C–H out of plane bending
GR/PANI nanocomposites synthesized in DMSO	1627.625	C=C of quinoid ring
	1528.573	C=C of benzoid ring
	1365.621	C–N of secondary amine
	1279.352	C=N (–N=Quinoid=N–)
	1196.278	C–H in-plane bending
	865.873	C–H out of plane bending
GR/PANI nanocomposites synthesized in DMC	1621.235	C=C of quinoid ring
	1522.185	C=C of benzoid ring
	1356.036	C–N of secondary amine
	1266.571	C=N (–N=Quinoid=N–)
	1193.082	C–H in-plane bending
	889.541	C–H out of plane bending
GR/PANI nanocomposites synthesized in acetone	1624.430	C=C of quinoid ring
	1525.380	C=C of benzoid ring
	1362.426	C–N of secondary amine
	1266.571	C=N (–N=Quinoid=N–)
	1199.473	C–H in-plane bending
	879.956	C–H out of plane bending
GR/PANI nanocomposites synthesized in THF	1624.430	C=C of quinoid ring
	1522.185	C=C of benzoid ring
	1359.231	C–N of secondary amine
	1272.962	C=N (–N=Quinoid=N–)
	1196.278	C–H in-plane bending
	892.737	C–H out of plane bending
GR/PANI nanocomposites synthesized in [BMIM][PF_6]	1624.430	C=C of quinoid ring
	1522.185	C=C of benzoid ring
	1359.231	C–N of secondary amine
	1263.376	C=N (–N=Quinoid=N–)
	1193.082	C–H in-plane bending
	812.582	C–H out of plane bending
	896.726	$[PF_6]^-$ vibrations

GR/PANI nanocomposites synthesized in [BMIM][NTF_2]	1639.997	C=C of quinoid ring
	1522.185	C=C of benzoid ring
	1365.621	C–N of secondary amine
	1221.839	C=N (–N=Quinoid=N–)
	1163.181	C–H in-plane bending
	809.777	C–H out of plane bending
	1071.666/ 1221.839	$–SO_3H$
GR/PANI nanocomposites synthesized in [BDMIM][BF_4]	1621.235	C=C of quinoid ring
	1522.235	C=C of benzoid ring
	1359.231	C–N of secondary amine
	1266.959	C=N (–N=Quinoid=N–)
	1193.082	C–H in-plane bending
	865.873	C–H out of plane bending
	1090.257	$[BF_4]^-$ vibrations
GR/PANI nanocomposites synthesized in [BMIM][BF_4]	1627.625	C=C of quinoid ring
	1519.390	C=C of benzoid ring
	1381.955	C–N of secondary amine
	1261.349	C=N (–N=Quinoid=N–)
	1199.473	C–H in-plane bending
	865.813	C–H out of plane bending
	1076.999	$[BF_4]^-$ vibrations

information for spectra obtained in other solvents are also presented in Table-2. Basically, the nanocomposites of graphene/polyaniline showed characteristic bands at about 1600, 1400, 1300 and 800 cm^{-1} which are attributed to the C=C, C-N and lastly C-H out of plane vibrations respectively [9,11,28,29,36-39]. It was obvious that a nanocomposite was formed due to the slight shift in the FTIR bands of the GR/PANI nanocomposites from those obtained for PANI alone. Two reasons have been adduced for these shift in bands (i) there is a hydrogen bonding between the PANI backbone and the O=C-O of GR and (ii) the π-π interaction between the two constituents of the nanocomposites [28,29,37,38].

Emergence of new IR peaks (not shown) was observed in the FTIR spectra recorded for the nanocomposites synthesized in ionic liquids. For example, in ionic liquid [BMIM][PF_6] a new peak around 970 cm^{-1} is attributed to the vibrations of the $[PF_6]^-$ anion [40]. Bands around 1220 and 1070 cm^{-1} are ascribed to $–SO_3H$ in the GR/PANI composites synthesized in [BMIM][NTF_2] [33]. Lastly, vibration modes of $[BF_4]^-$ anion was observed around 1040 cm^{-1} in the nanocomposites synthesized in [BDMIM]/[BMIM][BF_4] [40]. All these structural spectroscopic differences distinctively confirmed that the GR/PANI nanocomposite synthesized is different from one solvent to another as clearly supported by their different SEM morphology (Figs. 1-3).

Ultra violet visible spectroscopy: The UV-visible experiment was performed within the wavelength region of 100 to 1000 nm. The UV-visible spectrum of graphene oxide (not shown) is characterized by absorption bands at 223.55 and 256.87 nm attributed to the π→π* transition of the aromatic C-C bonds and the n→π* transition of the C=O bonds respectively [28,30]. After deoxygenation (or reduction) by hydrazine, the 256.87 nm peak shifted to higher wavelength 269.83 nm (Fig. 7a) due to the electronic transition (n→π* transition of C-O bonds) within the graphene molecule [30].

Fig. 7b shows the UV-visible spectrum of PANI with absorption bands at 313.33, 461.41 and 843.64 nm, attributed to the π→π* electronic transition of benzoid rings, polaron →π* and π→polaron electronic transitions respectively [28,29,38,39]. The first two peaks indicate the protonation of the PANI backbone while the last one indicates that the PANI is in the conductive state/form *i.e.* the emeraldine salt [39]. UV-visible spectroscopy is one of the most important techniques in the elucidation of the structural properties of the nanostructured conductive polymers. The bathochromic shifts that are encountered in these polymers shows that the energy gap of the nanosized conductive polymers is smaller than that of conventional conducting polymers making the nanosized have higher conductivity. These could be related to the extended conjugation, which is found in nanosized conductive polymer due to increased number of polarons in between the electronic bands [36].

The UV spectra of GR/PANI nanocomposites gave absorption peaks characteristics of both constituents (graphene and polyaniline) (Figs. 7c and d). Absorption peak around 254 nm correspond to the π→π* transition in the aromatic C-C of GR, while bands at about 361, 461 and 876 nm are ascribed to the π→π*, polaron→π* and π→polaron transitions in PANI respectively. Successful synthesis of the GR/PANI nanocomposite due to the interaction between GR and PANI was demonstrated by the disappearance of the GR absorption band at 222.16 nm and appearance of a new absorption band at 254.10 nm for GR/PANI nanocomposites in toluene (Fig. 7c). Successful synthesis of GR/PANI in [BMIM][PF_6] was also confirmed by the appearance of a new absorption band at 261.04 nm. Similar results are reported in literature [27,29,38]. The presence of the π→polaron transitions peak in nanocomposites confirms that even though PANI was exposed to hydrazine during graphene oxide reduction, the conductive form of PANI was recovered through the reoxidation/redoping processes. These UV-visible results are in good agreement with those of EDX and FTIR results.

Thermogravimettric analysis: The structural characteristics of graphene oxide, GR, PANI and GR/PANI nano-

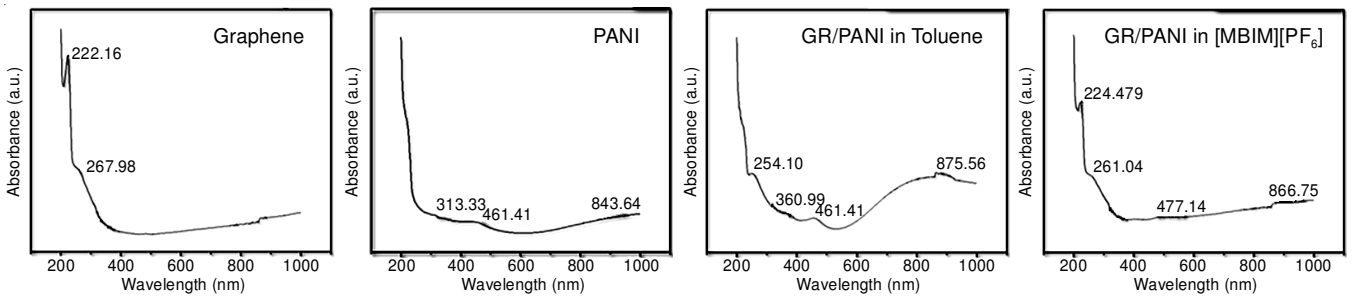

Fig. 7. UV-visible of PANI, GR and GR/PANI nanocomposites synthesized in toluene and [BMIM][PF_6]

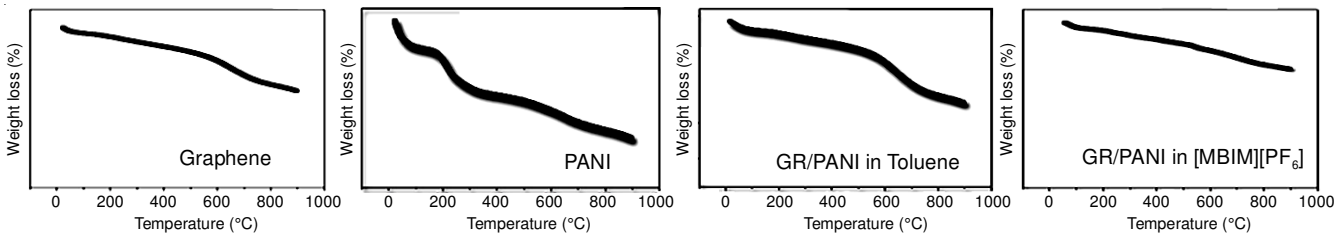

Fig. 8. TGA graphs of GR, PANI and GR/PANI nanocomposites synthesized in the presence of toluene and [BMIM][PF_6]

composites were studied by thermal analysis. The samples were heated from 0 to 900 °C at the heating rate of 10 °C/min and under nitrogen atmosphere (60 mL/min flow) using the ramp method.

Fig. 8 presents the TGA graphs of GR, PANI and GR/PANI nanocomposites synthesized in the presence of toluene and [BMIM][PF_6]. The TGA graph of graphene oxide (not shown) indicates that there is a small loss of weight at about 100 °C which can be correlated to the loss of intercalated water [9]. There is also a substantial weight loss starting from about 200 to 700 °C and this is attributed to the decomposition of all oxygen containing groups *i.e.* the pyrolysis of –OH, -CO and –COO groups [9,40,41]. The presence of these functional groups makes graphene oxide to be thermally unstable [40]. After reduction of graphene oxide at 98 °C by hydrazine, the resulting material (GR) lost some intercalation water around 100 °C and subsequent small weight loss from 100-600 °C (Fig. 8a). The small weight loss further confirmed the reduction of graphene oxide (deoxygenation) to GR due to significant removal of most of the oxygen moieties present in graphene oxide. The result agrees with the EDX, FTIR and UV-visible results, which indicate that not all the oxygen functional groups were completely removed during reduction [9].

Polyaniline undergoes thermal decomposition at around 100, 180-400 and 650-750 °C (Fig. 8b). These mass loses are caused by removal of water/and or absorbed moisture in the polymer back bone, loss of dopant ions in the form of $HCl_{(g)}$ and oligomers and finally the low molecular fragments, degradation and decomposition of the polymer itself [42,43].

The GR/PANI nanocomposites synthesized in both toluene (Fig. 8c) and ionic liquid [BMIM][PF_6] (Fig. 8d) also lost water of intercalation at about 100 °C and again at around 500-800 °C. This loss is attributed to the oxidative degradation of the composite itself [9,41,42]. There is no further weight loss after 800 °C because the residues left after degradation of the composites are inert materials such as carbonized polymer fragments and graphite. The thermal stability of the GR/PANI nanocomposites, which is shown by steady weight loss suggests that there is a good π-π interaction between graphitic monolayers and polyaniline nanostructures. This is in agreement with the FTIR and UV-visible results [41,42].

Conclusion

This study explored the synthesis and characterization of GR, PANI and GR/PANI nanocomposite. Effects of solvent on GR/PANI synthesis was investigated using both conventional organic solvents and green solvents (ionic liquids) which are safer chemicals and environmentally friendly. The synthesized nanocomposite was characterized using both microscopic and spectroscopic techniques. The SEM micrographs of GR/PANI nanocomposite synthesized using ionic liquids showed nucleated, agglomerated and evenly dispersed PANI nanofibre on the graphene sheets. The conventional organic solvents gave slippery wafers/flakes and passivated films or layers of PANI nanofibre on the graphene sheets. The XRD distinctively identified the crystalline nature of the nanocomposite prepared from both ionic liquids and conventional organic solvents. The crystal sizes range between 89-950 nm and 29-250 nm for the nanocomposite synthesized using ionic liquids and organic solvents respectively. FTIR, UV-visible, EDX and TGA results showed that the synthesized graphene wasn't completely reduced, while the remaining oxygen moieties aids its dispersion in different solvents used in this study (since completely reduced GR is highly hydrophobic). Results demonstrated that GR/PANI prepared using green solvents (ionic liquids) demonstrated properties such as crystallinity, thermal stability that compared very well with nanocomposite made using conventional organic solvents. Thus, it is strongly suggested that graphene/polyaniline nanohybrids and other related nanocomposites be prepared using ionic liquids (green solvents) as alternative to the presently used organic solvents as reaction media to save our environment from chemical pollution. The conductivity, rheology, photochemical and electrochemical properties of the synthesized GR/PANI nanocomposite and its potential application in catalysis, sensor and energy devices should be carried out.

ACKNOWLEDGEMENTS

The authors appreciated North-West University Chemistry Department and Prof. Eno Ebenso for providing conducive research platform to carry successfully out this study. Financial assistance was provided by the National Research Foundation, South Africa is gratefully acknowledged.

REFERENCES

1. M. Manoharan, *Technol. Soc.*, **30**, 401 (2008); https://doi.org/10.1016/j.techsoc.2008.04.016.
2. P.T. Anastas and M.M. Kirchhoff, *Acc. Chem. Res.*, **35**, 686 (2002); https://doi.org/10.1021/ar010065m.
3. G. Singh and A. Kumar, *Ind. J. Chem.*, **47A**, 495 (2008).
4. M.J. Earle and K.R. Seddon, *Pure Appl. Chem.*, **72**, 1391 (2000); https://doi.org/10.1351/pac200072071391.
5. B. Wu, W.W. Liu, Y.M. Zhang and H.P. Wang, *Chem. Eur. J.*, **15**, 1804 (2009); https://doi.org/10.1002/chem.200801509.
6. D. Han and K.H. Row, *Molecules*, **15**, 2405 (2010); https://doi.org/10.3390/molecules15042405.
7. T. Welton, *Chem. Rev.*, **99**, 2071 (1999); https://doi.org/10.1021/cr980032t.

8. L. Jiang, X.P. Shen, J.L. Wu and K.C. Shen, *J. Appl. Polym. Sci.*, **118**, 275 (2010); https://doi.org/10.1002/app.32278.
9. K. Zhang, L.L. Zhang, X. Zhao and J. Wu, *Chem. Mater.*, **22**, 1392 (2010); https://doi.org/10.1021/cm902876u.
10. O.K. Park, T. Jeevananda, N.H. Kim, S. Kim and J.H. Lee, *Scr. Mater.*, **60**, 551 (2009); https://doi.org/10.1016/j.scriptamat.2008.12.005.
11. D. Li and R.B. Kaner, *J. Am. Chem. Soc.*, **128**, 968 (2006); https://doi.org/10.1021/ja056609n.
12. S. Stankovich, R.D. Piner, X. Chen, N. Wu, S.B.T. Nguyen and R.S. Ruoff, *J. Mater. Chem.*, **16**, 155 (2006); https://doi.org/10.1039/B512799H.
13. N.A. Kotov, *Nature*, **442**, 254 (2006); https://doi.org/10.1038/442254a.
14. H. Shirakawa, E.J. Louis, A.G. MacDiarmid, C.K. Chiang and A.J. Heeger, *J. Chem. Soc. Chem. Commun.*, **16**, 578 (1977); https://doi.org/10.1039/c39770000578.
15. J. Huang, *Pure Appl. Chem.*, **78**, 15 (2006); https://doi.org/10.1351/pac200678010015.
16. A.S. Adekunle, J. Pillay and K.I. Ozoemena, *Electrochim. Acta*, **55**, 4319 (2010); https://doi.org/10.1016/j.electacta.2009.02.102.
17. C.K. Das and A. Mandal, *J. Mater. Sci. Res.*, **1**, 45 (2012).
18. H. Wang, Q. Hao, X. Yang, L. Lu and X.A. Wang, *Nanoscale*, **2**, 2164 (2010); https://doi.org/10.1039/c0nr00224k.
19. D.A. Skoog, F.J. Holler and S.R. Crouch, Instrumental Analysis, Brooks/Cole, Cengage Learning, edn 6 (2007).
20. C. Hammond, The Basics of Crystallography and Diffraction, International Union of Crystallography Texts on Crystallography: No. 3, (1997).
21. C. Hammond, Royal Microscopical Society Microscopy Handbooks: Introduction To Crystallography, Revised Edition, Oxford University Press, Oxford, UK (1992).
22. C. Harish, V.S. Sreeharsha, C. Santhosh, R. Ramachandran, M. Saranya, T.M. Vanchinathan, K. Govardhan and A.N. Grace, *Adv. Sci. Eng. Med.*, **5**, 140 (2013); https://doi.org/10.1166/asem.2013.1237.
23. W.L. Zhang, B.J. Park and H.J. Choi, *Chem. Commun.*, **46**, 5596 (2010); https://doi.org/10.1039/c0cc00557f.
24. Q. Li, B. Guo, J. Yu, J. Ran, B. Zhang, H. Yan and J.R. Gong, *J. Am. Chem. Soc.*, **133**, 10878 (2011); https://doi.org/10.1021/ja2025454.
25. C. Dhand, M. Das, G. Sumana, A.K. Srivastava, M.K. Pandey, C.G. Kim, M. Datta and B.D. Malhotra, *Nanoscale*, **2**, 747 (2010); https://doi.org/10.1039/b9nr00346k.
26. Y. Si and E.T. Samulski, *Chem. Mater.*, **20**, 6792 (2008); https://doi.org/10.1021/cm801356a.
27. C. Hontoria-Lucas, A. Lopez-Peinado, J.D. López-González, M. Rojas-Cervantes and R. Martin-Aranda, *Carbon*, **33**, 1585 (1995); https://doi.org/10.1016/0008-6223(95)00120-3.
28. S. Goswami, U. Maiti, S. Maiti, S. Nandy, M. Mitra and K. Chattopadhyay, *Carbon*, **49**, 2245 (2011); https://doi.org/10.1016/j.carbon.2011.01.055.
29. S. Ameen, M.S. Akhtar and H.S. Shin, *Sensors Actuators B: Chem.*, 173, 177 (2012); https://doi.org/10.1016/j.snb.2012.06.065.
30. F. Thema, M. Moloto, E. Dikio, N. Nyangiwe, L. Kotsedi, M. Maaza and M. Khenfouch, *J. Chem.*, Article ID 150536 (2012) https://doi.org/10.1155/2012/150536.
31. Q. Hao, H. Wang, X. Yang, L. Lu and X. Wang, *Nano Res.*, **4**, 323 (2011); https://doi.org/10.1007/s12274-010-0087-4.
32. P. Blake, E.W. Hill, A.H. Castro Neto, K.S. Novoselov, D. Jiang, R. Yang, T.J. Booth and A.K. Geim, *Appl. Phys. Lett.*, **91**, 063124 (2007); https://doi.org/10.1063/1.2768624.
33. S. Pisana, M. Lazzeri, C. Casiraghi, K.S. Novoselov, A.K. Geim, A.C. Ferrari and F. Mauri, *Nat. Mater.*, **6**, 198 (2007); https://doi.org/10.1038/nmat1846.
34. Z. Chen, Y. Lin, Y.M.J. Rooks and P. Avouris, *Physica E*, **40**, 228 (2007); https://doi.org/10.1016/j.physe.2007.06.020.
35. S. Stankovich, D.A. Dikin, R.D. Piner, K.A. Kohlhaas, A. Kleinhammes, Y. Jia, Y. Wu, S.B.T. Nguyen and R.S. Ruoff, *Carbon*, **45**, 1558 (2007); https://doi.org/10.1016/j.carbon.2007.02.034.
36. Deepshikha and T. Basu, *Anal. Lett.*, **44**, 1126 (2011); https://doi.org/10.1080/00032719.2010.511734.
37. S. Liu, X. Liu, Z. Li, S. Yang and J. Wang, *New J. Chem.*, **35**, 369 (2011); https://doi.org/10.1039/C0NJ00718H.
38. Y. Li, H. Peng, G. Li and K. Chen, *Eur. Polym. J.*, **48**, 1406 (2012); https://doi.org/10.1016/j.eurpolymj.2012.05.014.
39. H. Mi, X. Zhang, S. Yang, X. Ye and J. Luo, *Mater. Chem. Phys.*, **112**, 127 (2008); https://doi.org/10.1016/j.matchemphys.2008.05.022.
40. X. Du, M. Xiao and Y. Meng, *J. Polym. Sci., B, Polym. Phys.*, **42**, 1972 (2004); https://doi.org/10.1002/polb.20102.
41. N.A. Kumar, H. Choi, Y.R. Shin, D.W. Chang, L. Dai and J. Baek, *ACS Nano*, **6**, 1715 (2012); https://doi.org/10.1021/nn204688c.
42. G. Gheno, B. de Souza, N. Regina and R. Hübler, *Macromol. Symp.*, **299-300**, 74 (2011); https://doi.org/10.1002/masy.200900137.
43. M. Kulkarni, B. Kale, S. Apte, S. Naik, U. Mulik and D. Amalnerkar, *Chem. Chemical Technol.*, **5**, 55 (2011).